Solidification Behavior in Newly Designed Ni-Rich Ni-Ti-Based Alloys

SUMANTA SAMAL, KRISHANU BISWAS, and GANDHAM PHANIKUMAR

The present investigation reports phase and microstructure evolution during solidification of novel Ni-rich Ni-Ti-based alloys, $Ni_{60}Ti_{40}$, $Ni_{50}Cu_{10}Ti_{40}$, $Ni_{48}Cu_{10}Co_2Ti_{40}$, and $Ni_{48}Cu_{10}Co_2Ti_{38}Ta_2$ during suction casting. The design philosophy of the multicomponent alloys involves judicious selection of alloying elements such as Cu, Co, and Ta in the near $Ni_{60}Ti_{40}$ eutectic alloy by replacing both Ni and Ti so that phase mixture in the microstructure remains the same from the binary to quinary alloy. The basic objective is to study the effect of addition of Cu, Co, and Ta on the phase evolution and transformation in the Ni-rich Ni-Ti-based alloys. The detailed electron microscopic studies on these suction cast alloys reveal the presence of ultrafine eutectic lamellae between NiTi and Ni_3Ti phases along with dendritic NiTi and Ti_2Ni phases. It has also been observed that in the binary ($Ni_{60}Ti_{40}$) alloy, the ordered NiTi (B2) phase transforms to trigonal (R) phase followed by NiTi martensitic phase (M-phase), *i.e.,* B2 → R-phase → M-phase during solid-state cooling. However, the addition of alloying elements such as Cu, Co to the binary ($Ni_{60}Ti_{40}$) alloy suppresses the martensitic transformation of the ordered NiTi (B2) dendrite. Thus, in the ternary and quaternary alloys, the ordered NiTi (B2) phase is transformed to only trigonal (R) phase, *i.e.,* B2 → R-phase. The secondary precipitate of Ti_2Ni has been observed in all of the studied alloys. Interestingly, $Ni_{48}Cu_{10}Co_2Ti_{38}Ta_2$ quinary alloy shows the disordered nature of NiTi dendrites. The experimentally observed solidification path is in good agreement with Gulliver–Scheil simulated path for binary alloy, whereas simulated solidification path deviates from the experimental results in case of ternary, quaternary, and quinary alloys.

DOI: 10.1007/s11661-016-3789-8

I. INTRODUCTION

OVER the past few decades, Ni-Ti alloys (Nitinol)[1–4] have extensively been researched due to existence of the unique and improved properties including high strength at elevated temperature, good workability, excellent corrosion resistance, shape memory effect, *etc.* The search for novel advanced materials with better mechanical properties has led to continuous drive in the scientific community.[5] Recently, it has been reported[6–9] that bulk nano/ultrafine eutectic alloy with micron-scale dendritic phases is a promising material; exhibiting improved and well-balanced combination of strength and ductility required for niche applications. Sufficiently large number of studies has been reported in the literature on the development of these types of composite microstructure in Ti-based multicomponent alloys such as Ti-Fe-Sn,[10–12] Ti-Fe-Co,[13,14] Ti-Cu-Ni-Sn-Nb/Ta[6,15,16] by proper selection of the alloying elements and their concentration. However, very limited studies[17–19] have been reported on the Ni-based multicomponent alloys so far. To the best of the authors' knowledge, the equilibrium Ni-rich Ni-Ti-based multicomponent alloy phase diagram is not available, and thus, it is very tedious to predict the phase formation and microstructure evolution in the Ni-rich Ni-Ti-based multicomponent alloys. Therefore, one needs to investigate systematically the effect of addition of alloying elements to near-eutectic Ni-Ti binary alloy (as indicated by dotted line in Figure 1) with an aim to obtain clear understanding of the phase formation in these alloys. It is to be noted that the detailed mechanical properties of Ni-rich Ni-Ti-based alloys has been reported in the earlier publication (Table I),[20] revealing that fine tuning the composition by addition of alloying elements in the alloy would lead well-balanced mechanical properties (ultimate strength ~2 GPa and ductility ~13 pct).

The objective of the current investigation is to explore the novel approach to achieve in-depth understanding of the phase formation and microstructure evolution of the investigated Ni-rich Ni-Ti-based alloys by the systematic addition of different alloying elements such as Cu, Co, and Ta in the Ni-rich Ni-Ti binary alloy. The purpose of

SUMANTA SAMAL, formerly Ph.D. Student with the Department of Materials Science and Engineering, Indian Institute of Technology Kanpur, Kanpur, Uttar Pradesh 208016, India, is now Institute Postdoctoral Fellow with the Department of Metallurgical and Materials Engineering, Indian Institute of Technology Madras, Chennai, Tamil Nadu 600036, India. KRISHANU BISWAS, Professor, is with the Department of Materials Science and Engineering, India Institute of Technology Kanpur. Contact e-mail: kbiswas@iitk.ac.in GANDHAM PHANIKUMAR, Professor, is with the Department of Metallurgical and Materials Engineering, Indian Institute of Technology Madras.

Manuscript submitted April 20, 2016.
Article published online October 4, 2016

the present manuscript is to understand the solidification behavior of the multicomponent Ni-Ti-Co-Ta-Cu alloy. Earlier, we have reported that the unique mechanical properties of the as-cast quinary alloy consist of nanoscale eutectic between NiTi and Ni_3Ti along with dendrites of NiTi and Ti_2Ni.[20] Therefore, the present manuscript is aimed at understanding microstructural evolution and solidification pathways. In order to understand the solidification pathways, we have utilized arc melting cum suction casting in copper mold, akin to Bridgman-like directional solidification technique. Using binary to quinary alloys, we have symmetrically studied the solidification behavior of these alloys. In addition, the solidification pathways of all the investigated Ni-rich Ni-Ti-based alloys are simulated by two analytical solidification models such as Lever rule and Gulliver–Scheil models using CALPHAD method with the help of ThermoCalc® software packages and TCNI8® database and finally compared with the experimental results of these alloys.

II. EXPERIMENTAL DETAILS

The Ni-rich Ni-Ti-based alloys were prepared by arc melting the elements (99.9 pct purity) in the required proportion under high-purity argon atmosphere. The alloy was remelted at least 5 times to ensure chemical homogeneity. The alloy was then subsequently suction cast in a water-cooled split copper mold to obtain cylindrical specimen with ϕ = 3 mm diameter and aspect ratio of 17:1. The microstructural characterization of all the investigated alloys was carried out by scanning electron microscope (Model: Carl Zeiss EVO 50, SEM) coupled with an energy dispersive spectroscopy (EDS, INCA PENTA FET X3) and transmission electron microscope (TEM, FEI G^2 with high-resolution capabilities). The foils for TEM observation was prepared by standard ion milling preparation technique. The thermodynamic simulations on the solidification pathways of the investigated Ni-rich Ni-Ti-based alloys was carried out by ThermoCalc® software using TCNI8® database to explain the phase evolution during solidification. The solidification pathways were predicted using Scheil solidification simulation in graphical mode of commercially available ThermoCalc® software, and finally, the predicted results were validated with the experimental results.

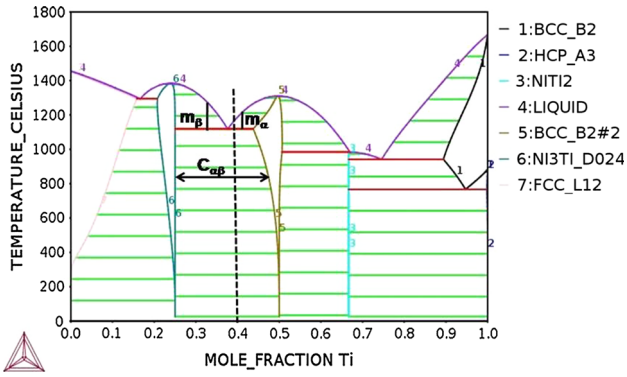

Fig. 1—Phase diagram of the Ni-Ti binary alloy generated by ThermoCalc® software using TCNI8 database. The dotted line in figure denotes the composition of studied $Ni_{60}Ti_{40}$ alloy (Ni-rich part of Ni-Ti phase diagram).

III. DESIGN METHODOLOGY FOR NANOSCALE/ ULTRAFINE Ni-RICH Ni-Ti-BASED EUTECTIC ALLOYS

Eutectic alloys are technologically important class of materials due to easy processing as well as possibility of obtaining good combination of mechanical properties. The salient length scale for eutectic microstructure is the interlamellar spacing (λ). The yield strength for two-phase eutectic alloy is related to the interlamellar spacing (λ), according to Hall–Petch-type equation,[21] *i.e.*, $\sigma_{ye} = \sigma_{0e} + K_H\lambda^{(-1/2)}$, where σ_{ye} is the yield strength of the material, σ_{0e} is the friction stress, λ is the interlamellar spacing, and K_H is Hall–Petch slope.[21] Therefore, it is necessary to reduce the interlamellar spacing (λ) in order to obtain high strength. The strength of the eutectic alloys can substantially be increased by reducing λ to nanometric regime. However, these alloys primarily consisting of fine eutectic microstructure exhibit poor ductility.[22] Thus, these alloys are designed in such a way that the microstructure consists of eutectic with primary dendrites.[21] This type of microstructure leads to substantial improvement in ductility because of the presence of the dendrites. In the present study, Ni-rich Ni-Ti-based multicomponent alloys have been designed from the near-eutectic binary $Ni_{60}Ti_{40}$ alloy (marked as dotted line in Figure 1) in such a way that the phase mixture remains almost the same from binary to higher order alloy system. The ternary, quaternary, as well as quinary alloying addition are meant to reduce λ without changing the phase mixture present in the binary alloy. Therefore, alloying

Table I. Mechanical Properties of the Investigated Ni-Rich Ni-Ti-Based Alloys.[20]

Alloys	Elastic Strain (ε_e) (Percent)	Yield Strength (σ_y) (MPa)	Ultimate Compressive Strength (σ_{UCS}) (MPa)	Fracture Strength (σ_f) (MPa)	Plasticity (ε_P) (Percent)	Plasticity Corresponding to UCS (Percent)	Interlamellar Spacing (λ) (nm)
$Ni_{60}Ti_{40}$	0.48	79.4	841	841	4.2	4.2	125 ± 5
$Ni_{50}Cu_{10}Ti_{40}$	0.35	68.9	1257	1257	4.7	4.7	113 ± 6
$Ni_{48}Cu_{10}Co_2Ti_{40}$	0.92	195.6	1815	1815	7.7	7.7	84 ± 2
$Ni_{48}Cu_{10}Co_2Ti_{38}Ta_2$	0.66	172.7	1988.8	1929.7	13.5	11.9	75 ± 4

elements need to be selected judiciously. The alloying elements Cu, Co, and Ta have been systematically substituted in Ni or Ti so that all the alloying elements form the isomorphous phase diagram with Ni or Ti and therefore the pseudo-Ni(Cu, Co)-Ti(Ta) alloys are designed to obtain the similar phase mixture. Under equilibrium conditions, the binary $Ni_{60}Ti_{40}$ alloy consists of eutectic between NiTi and Ni_3Ti phases with primary NiTi dendrites.

A deep eutectic with a plunging liquidus is observed for $Ni_{60}Ti_{40}$ alloy in Ni-Ti phase diagram. The addition of multiple components in the binary alloy renders the subsequent eutectic growth more sluggish, favoring the ultrafine or nanoscale interlamellar spacing (λ). A semi-quantitative analysis can be used in the present study to obtain eutectic alloy system with finer eutectic lamellae. According to Jackson–Hunt (JH) model,[23–25] the eutectic solidification front velocity (V) and interlamellar spacing (λ) are related by the following equation:

$$V^{1/2}\lambda = A, \qquad [1]$$

where A is given by

$$A = \frac{K_2}{K_1}, \qquad [2]$$

where K_1 and K_2 are provided by the following relationships:

$$K_1 = \frac{m_V C_{\alpha\beta} P}{D f_\alpha f_\beta} \qquad [3]$$

and

$$K_2 = 2m_V \sum_i \frac{\Gamma_i \sin\theta_i}{m_i^V f_i};\ (i = \alpha, \beta), \qquad [4]$$

where m_V is velocity-dependent liquidus slope, $C_{\alpha\beta}$ is the compositional range of the eutectic, D is the diffusion coefficient, the angles θ_i s are the contact angles between the solid phases (α and β phases) and liquid at the triple point, Γ_i s are the capillarity constants, which is defined by the ratio of surface energy to melting entropy per unit volume, and f_i s are the volume fractions of the solid phases in the microstructure at the growth temperature.

m_V is calculated using liquidus slopes of the individual phases:

$$\frac{1}{|m_V|} = \frac{1}{|m_\alpha|} + \frac{1}{|m_\beta|}, \qquad [5]$$

where m_α and m_β are the liquidus slopes of α and β phases in a eutectic system.

$$P = \sum_{n=1}^{\infty} \left(\frac{1}{n\pi}\right)^2 [\sin(n\pi f)]^2 \frac{P_n}{)1 + P_n^2 - 1 + 2K(V)}, \qquad [6]$$

$$\text{where } P_n = \left(2n\pi/P_e\right) \text{ and } P_e = V\lambda/2D. \qquad [7]$$

The first two factors on the right-hand side of Eq. [6] were derived by Jackson-Hunt[23] but the third factor was introduced by Trivedi *et al.*[24] for $P_e > 1$.

It is evident from the above equations that the λ depends upon the parameters such as (i) liquidus slope (m_α and m_β), (ii) coefficient of diffusion (D), (iii) eutectic range ($C_{\alpha\beta}$), and (iv) contact angles (θ). The higher absolute values of m_α and m_β will lead to small value of A and hence the interlamellar spacing will decrease. A is also influenced by the coefficient of diffusion. The diffusion coefficient in the liquid is considered to be of the order of 10^{-9} m^2/s. In the multicomponent systems, the addition of more substitutional solid solution forming elements will make diffusion very difficult. As a result, the value of A will be even smaller and hence cause even smaller value of λ for a given value of V. Therefore, this design concept gives rise to an idea for obtaining nanoscale or ultrafine eutectic spacing upon casting, by proper selection of alloying elements and their composition. A rather deep eutectic with plunging liquidus in the binary or ternary systems will provide the right candidate to obtain lower value A. The addition of quaternary and quinary alloying elements will also render subsequent eutectic growth more sluggish, favoring the nanoscale λ.

IV. RESULTS

A. *Microstructural Characterization*

The detailed microstructural characterization of the as-cast samples has been carried out using scanning electron microscopy (SEM). It is important to note that the SEM micrographs of the investigated alloys are obtained using backscattered electron (BSE) imaging mode to identify the different phases in the microstructure distinctly. SEM micrograph of the binary $Ni_{60}Ti_{40}$ alloy is shown in Figure 2(a). The inset shows the high-magnification image, indicating the presence of micron-sized NiTi dendrites (gray contrast) and Ti_2Ni (black contrast) phases along with eutectic between NiTi and Ni_3Ti phases. The microstructure of ternary alloy ($Ni_{50}Cu_{10}Ti_{40}$) (shown in Figure 2(b) with the inset revealing higher magnification micrograph) shows the presence of coarse dendritic Ti_2Ni and finer NiTi phases as well as eutectic between NiTi and Ni_3Ti. It is also found that the volume fraction of eutectic phase mixture increases significantly by addition of Cu in the Ti-Ni binary alloy. The SEM micrographs of the quaternary ($Ni_{48}Cu_{10}Co_2Ti_{40}$) and quinary ($Ni_{48}Cu_{10}Co_2Ti_{38}Ta_2$) alloys (as shown in Figures 2(c) and (d)) reveal the presence of coarse Ti_2Ni and finer NiTi phases along with fine-scale eutectic between NiTi and Ni_3Ti phases. It is evident that the eutectic forms bulk of the microstructure in all these alloys.

The detailed TEM investigation of all the investigated Ni-rich Ni-Ti-based alloys has been carried out to decipher the phases formed as well as their size and distribution in the microstructure. However, the representative TEM micrographs of the studied alloys are being provided here. The TEM bright-field micrograph of the $Ni_{60}Ti_{40}$ alloy (shown in Figure 3) reveals the presence of different phases, *i.e.,* ordered body-centered cubic NiTi (B2) dendritic phase, martensite (M) phase,

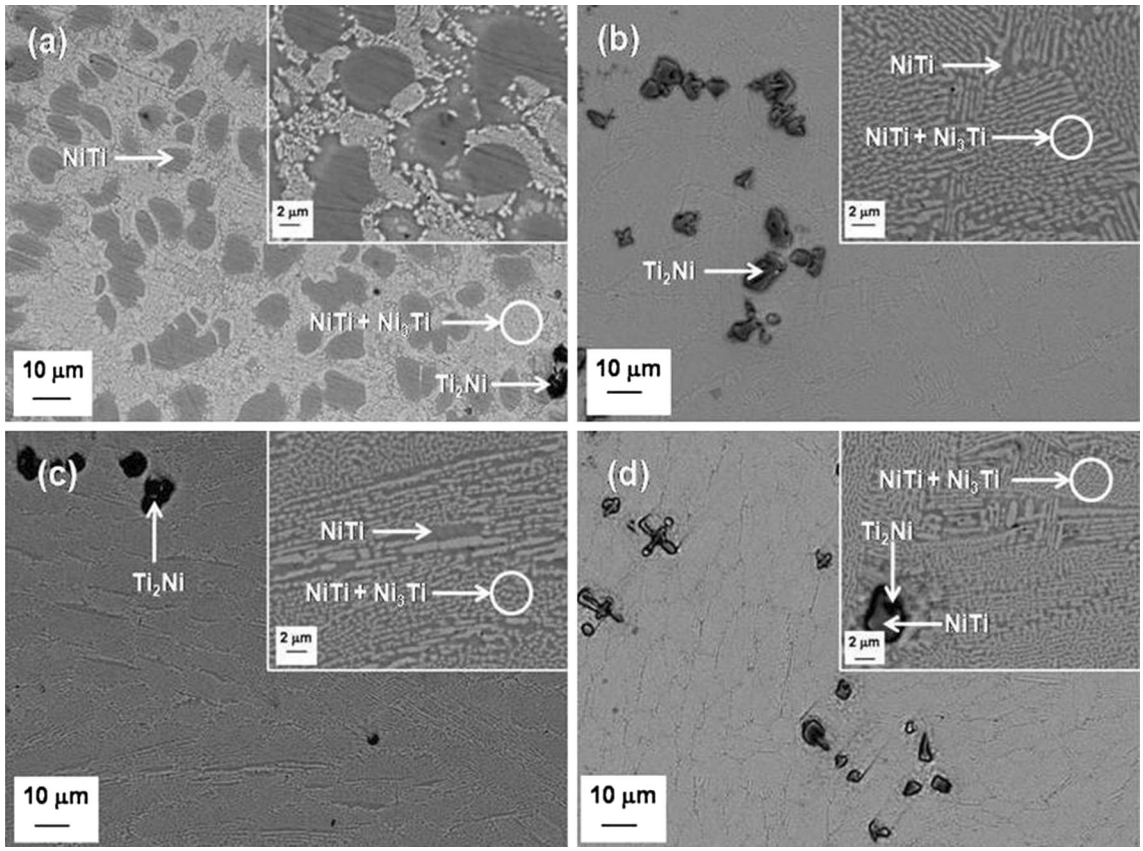

Fig. 2—BSE-SEM micrographs of the studied Ni-rich Ni-Ti-based alloys: (*a*) $Ni_{60}Ti_{40}$; (*b*) $Ni_{50}Cu_{10}Ti_{40}$; (*c*) $Ni_{48}Co_2Cu_{10}Ti_{40}$; and (*d*) $Ni_{48}Co_2Cu_{10}Ti_{38}Ta_2$. The inset in each figure shows higher magnification micrograph.

and trigonal (R) phase as well as eutectic between NiTi and Ni_3Ti phases. The constituent phases in the microstructure of $Ni_{60}Ti_{40}$ alloy are identified using selected area diffraction (SAD) patterns (shown in Figure 3) obtained from each phase.[20] It is to be noted that the martensite (M) phase is characterized by internal twinning. It has been reported[26,27] that the low-temperature martensite (M) phase is formed from the high-temperature ordered NiTi parent phase in this alloy.

The TEM bright-field micrograph of the ternary alloy ($Ni_{50}Cu_{10}Ti_{40}$) and corresponding SAD patterns of the constituent phases are shown in Figure 4. It reveals the presence of the ordered cubic NiTi (B2) phase and R-phase as well as eutectic between NiTi and Ni_3Ti phases. The finer precipitates of the trigonal (R) phase are also observed. It is to be noted that the formation of R-phase is attributed to the presence of Ni_4Ti_3 precipitate in the ordered NiTi phase as reported in the open literature.[28] The trigonal phase (*i.e.,* R-phase) is also reported to be incommensurate with the high-temperature austenitic NiTi (B2) phase. It has been reported in the literature[29] that the incommensurate diffuse scattering is attributed to the presence of nanoscale domain-like structure in the parent ordered austenitic NiTi (B2) phase. However, the diffuse scattering has not been observed in the present studied alloys, whereas the nanoscale domain-like structure has been revealed in the microstructure (Figure 4(c)) which leads to the formation of superlattice spots in the R-phase (SAD pattern of R-phase in Figure 4). The microstructure of R-phase is also characterized by the nucleation of the lenticular-shaped precipitate (shown in Figure 5(c)) from the defects region in the high-temperature austenitic NiTi (B2) phase and subsequent formation of self-accommodated microstructure due to growth mechanism. The R-phase transformation being first-order transformation is generally observed in the superplasticity and shape memory effect.

The TEM bright-field micrograph of quaternary ($Ni_{48}Cu_{10}Co_2Ti_{40}$) alloy (shown in Figure 5) reveals the presence of the phases such as NiTi (B2) phase, R-phase, and Ti_2Ni phases along with eutectics between NiTi and Ni_3Ti phases. Figure 5(b) shows the bright-field TEM micrograph of Ti_2Ni phase surrounded by eutectic lamellae. It is to be noted that the lenticular-shaped precipitates (*i.e.*, Ni_4Ti_3 precipitate) in the R-phase has also been observed (Figure 5(c)) in this alloy and the corresponding dark-field image is shown in Figure 5(d). The corresponding SAD patterns obtained from each phase in the microstructure of the alloy are provided in Figure 5. It has also been observed that the superlattice spots are present at a distance of 1/3 of the fundamental reflection, which is attributed to the presence of Ni_4Ti_3 precipitate in the ordered NiTi matrix phase. The detailed analysis of the SAD pattern from the eutectic lamellae indicates that the eutectic consists of B2 ordered NiTi and Ni_3Ti (Figure 5).

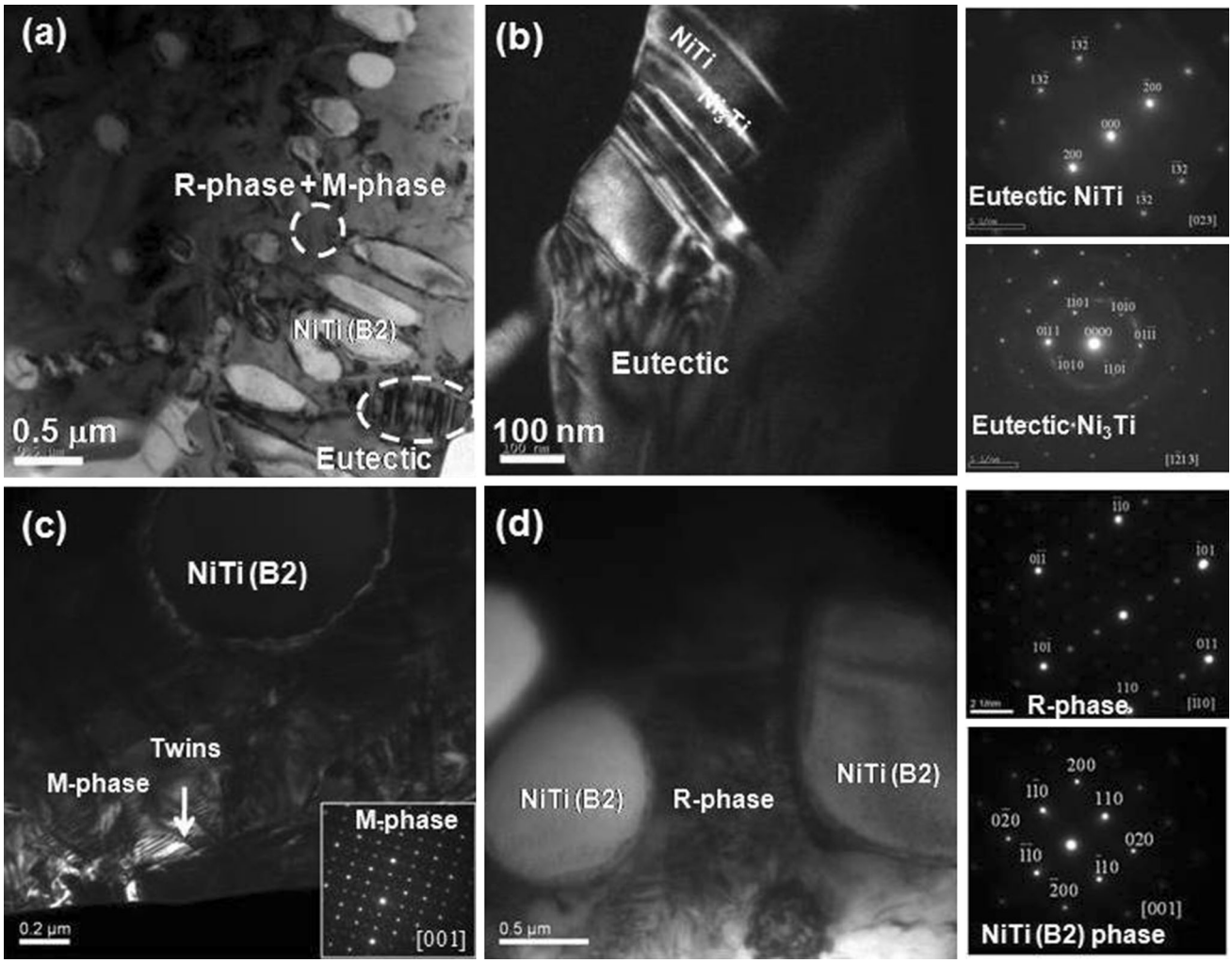

Fig. 3—TEM micrograph of $Ni_{60}Ti_{40}$ alloy: (*a*) bright-field micrograph showing overall features, (*b*) dark-field micrograph of eutectic region, (*c*) dark-field micrograph of M-phase and B2-phase, (*d*) bright-field micrograph showing R-phase and B2-phase.

TEM bright-field micrograph of the quinary $Ni_{48}Cu_{10}Co_2Ti_{38}Ta_2$alloy (as shown in Figure 6) shows the presence of micron-sized NiTi and Ti_2Ni phases along with fine-scale eutectic lamellae between B2-ordered NiTi and Ni_3Ti phases. It is important to note that the SAD pattern from NiTi dendritic phase is disordered in nature.

B. *Thermodynamic Simulations on Solidification Path*

The thermodynamic simulations of the investigated Ni-rich Ni-Ti-based alloys were carried out using Scheil solidification simulation in graphical mode of commercially available ThermoCalc® software to predict solidification pathways. The solidification pathways according to Lever rule model for binary $Ni_{60}Ti_{40}$ alloy (Figure 7(a)) can be described as L → L + BCC_B2 → BCC_B2 (*i.e.*, L → L + NiTi → NiTi). However, Gulliver–Scheil model shows the corresponding solidification pathways as L → L + BCC_B2→ L + BCC_B2 + Ni3Ti_D024 → BCC_B2 + Ni3Ti_D024 (*i.e.*, L → L + NiTi → L + NiTi + Ni_3Ti → NiTi + Ni_3Ti).

Similarly, the solidification pathways following Lever rule model for ternary $Ni_{50}Cu_{10}Ti_{40}$ alloy (Figure 7(b)) is expressed as L → L + BCC_B2 → BCC_B2 (*i.e.*, L → L + NiTi → NiTi). However, Gulliver–Scheil model shows the corresponding solidification pathways for the investigated ternary $Ni_{50}Cu_{10}Ti_{40}$ alloy as L → L + BCC_B2 → L + BCC_B2 + Ni3Ti_D024 → L + BCC_B2 + Cu2Ti + Ni3Ti_D024 → BCC_B2 + Cu2Ti + Ni3Ti_D024 (*i.e.*, L → L + NiTi → L + NiTi + Ni_3Ti → L + NiTi + Cu_2Ti + Ni_3Ti → NiTi + Cu_2Ti + Ni_3Ti). The similar type of solidification sequence for quaternary $Ni_{48}Cu_{10}Co_2Ti_{40}$ alloy (shown in Figure 7(c)) and quinary $Ni_{48}Cu_{10}Co_2Ti_{38}Ta_2$ alloy (shown in Figure 7(d)) has been found.

V. DISCUSSION

A. *Phase Transformation Behavior of Ni-Rich Ni-Ti-Based Alloys*

The solidification behavior of binary alloy having dilute concentration of alloying element is sufficiently

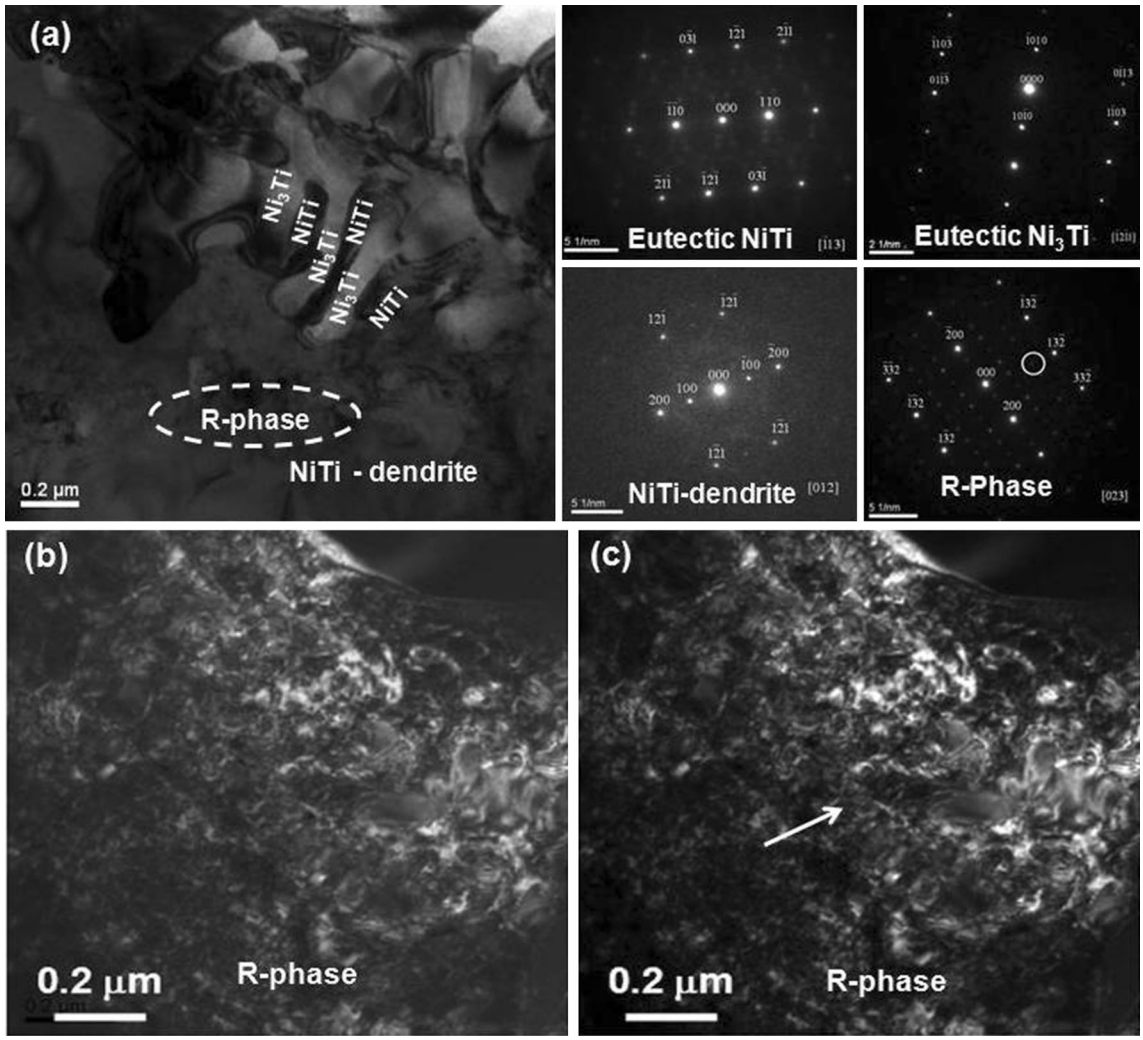

Fig. 4—TEM micrograph of $Ni_{50}Cu_{10}Ti_{40}$ alloy: (*a*) bright-field TEM micrograph revealing overall features, (*b*) bright-field micrograph of R-phase, (*c*) dark-field micrograph of R-phase.

documented in the literature.[30] However, studies on the phase formation in the multicomponent alloys are scarce and also less understood from both theoretical and experimental stand points. Therefore, studies on phase transformation behavior of the investigated novel Ni-rich Ni-Ti-based multicomponent alloys have both fundamental importance as well as practical implications. The understanding of phase transformation behavior requires detailed analyses of phases formed and careful analysis of microstructural features. In the following section, the phase transformation behavior of all the investigated Ni-rich Ni-Ti-based alloys has been discussed based upon SEM and TEM results.

The binary ($Ni_{60}Ti_{40}$) alloy consists of ordered NiTi phase, R-phase, and M-phase and Ti_2Ni phase along with eutectic between NiTi and Ni_3Ti phases. In this alloy system, the solidification pathways are (i) $L \rightarrow L + NiTi$, (ii) $L \rightarrow NiTi + Ni_3Ti$, (iii) $NiTi \rightarrow Ti_2Ni + Ni_3Ti$, *i.e.*, NiTi phase undergoes eutectoid transformation to form Ti_2Ni and Ni_3Ti phases, and (iv) finally, B2 $\rightarrow$ R-phase $\rightarrow$ M-(monoclinic B19′) phase, *i.e.*, the high-temperature austenitic ordered NiTi (B2) phase undergoes solid-state transformation to form martensitic (M) phase *via* trigonal (R) phase. The cooling rate (~100 K/s) during casting is not high enough to avoid such solid-state transformation. Similar type of solid-state phase transformation in NiTi alloy has also been observed by other investigators.[31–34]

Electron microscopic (SEM and TEM) results of ternary ($Ni_{50}Cu_{10}Ti_{40}$) alloy show the presence of NiTi (B2- and R-phases) and Ti_2Ni phases along with eutectic between NiTi and Ni_3Ti phases. In this alloy system, the M-phase has not been observed. This means that the addition of Cu as alloying element in the binary alloy suppresses the formation of M-phase. Thus, the solidification pathways of ternary ($Ni_{50}Cu_{10}Ti_{40}$) alloy are explained as follows: (i) $L \rightarrow L + NiTi$, (ii) $L \rightarrow NiTi + Ni_3Ti$, (iii) $NiTi \rightarrow Ti_2Ni + Ni_3Ti$, *i.e.,* NiTi phase *via* eutectoid transformation to form Ti_2Ni and Ni_3Ti phases, and (iv) finally, B2 $\rightarrow$ R-phase, *i.e.,* the parent ordered body-centered cubic NiTi (B2) phase undergoes solid-state transformation to form trigonal

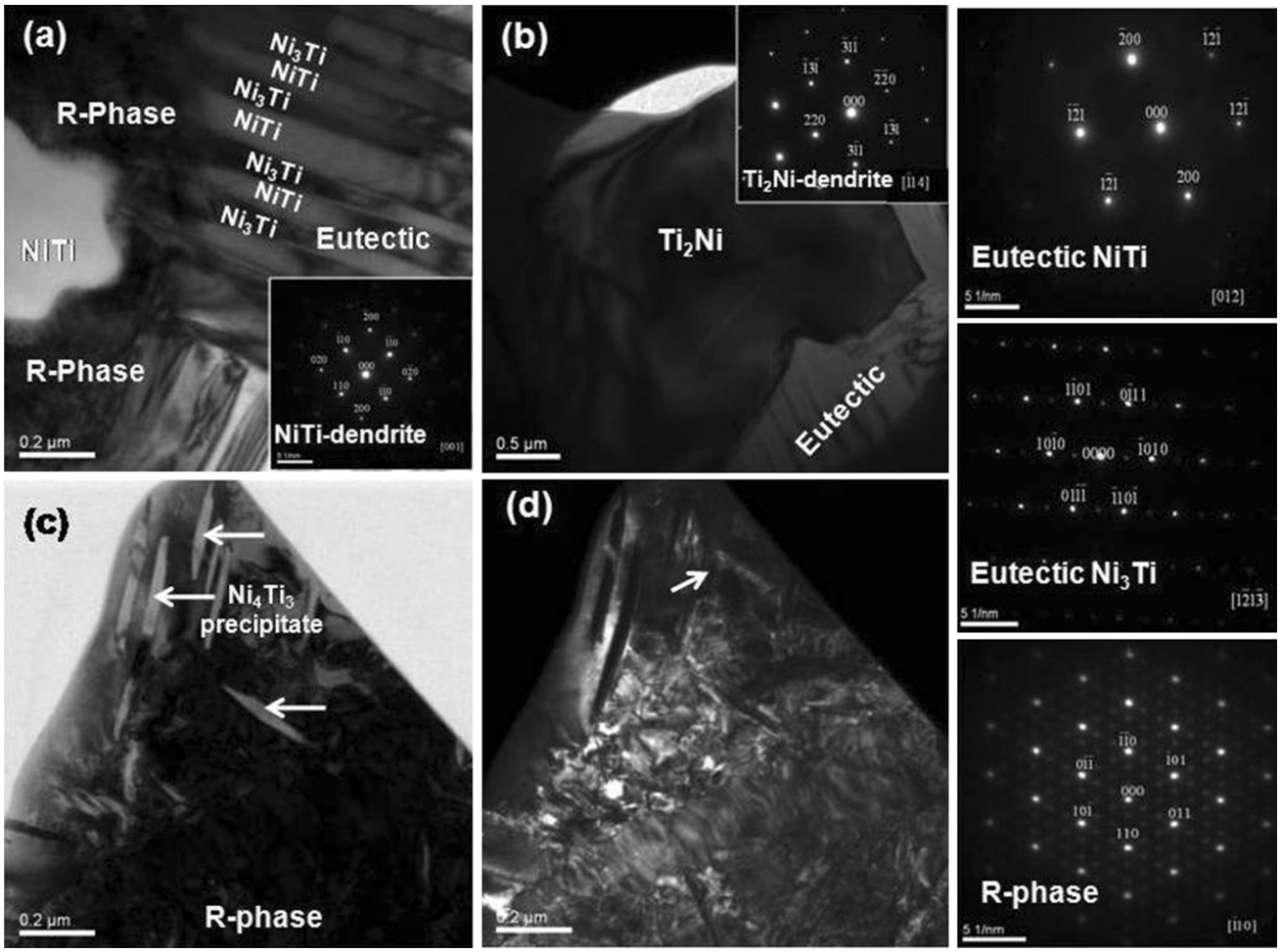

Fig. 5—TEM micrograph $Ni_{48}Cu_{10}Co_2Ti_{40}$ alloy: (*a*) bright-field micrograph showing overall features, (*b*) bright-field micrograph of Ti_2Ni phase surrounded by eutectic, (*c*, *d*) TEM micrograph of R-phase in bright-field and dark-field imaging mode, respectively.

(R) phase only. The solidification pathways for quaternary ($Ni_{48}Cu_{10}Co_2Ti_{40}$) alloy are same as that of the ternary ($Ni_{50}Cu_{10}Ti_{40}$) alloy. Hence, two-step phase transformation, *i.e.,* B2 → R-phase → M-(monoclinic B19′) phase, is observed in the binary alloy, whereas ternary ($Ni_{50}Cu_{10}Ti_{40}$) and quaternary ($Ni_{40}Cu_{10}Co_2Ti_{40}$) alloys exhibit only one-step phase transformation, *i.e.,* B2 → R-phase. Similar types of phase transformation have been reported by Buenconsejo *et al.*[35] and the two-step and one-step phase transformations are attributed to large and small grain size, respectively.

While quinary alloy ($Ni_{48}Cu_{10}Co_2Ti_{38}Ta_2$) consists of different micron-sized phases, *i.e.*, disordered NiTi phase and Ti_2Ni phase along with eutectic between NiTi and Ni_3Ti phases. The solidification pathways for quinary alloy are given as (i) L → L + NiTi, (ii) L → NiTi + Ni_3Ti, and (iii) finally, NiTi → Ti_2Ni + Ni_3Ti, *i.e.,* NiTi phase undergoes solid-state transformation to form Ti_2Ni and Ni_3Ti phases. In the quinary alloy, no further solid-state transformation has been observed. The detailed phase transformation of all the investigated alloys, *i.e.,* from binary to quinary alloys are provided in Table II.

B. *Thermodynamic Phase Prediction of Ni-Rich Ni-Ti-Based Alloys*

In the following, the solidification pathways and microstructural evolution will be discussed in the light of available literature. Using different solidification models, efforts have been made to explain the phase formation and microstructure evolution. Two classical solidification models such as Lever rule and Gulliver–Scheil models[36] have been employed to predict the solidification pathways during solidification of the investigated alloys using CALPHAD method with the aid of ThermoCalc® software packages and TCNI8® database. The Lever rule model predicts the equilibrium solidification path considering complete mixing of solutes in both solid and liquid. The basic solute balance equation in this model[36] can be expressed as $C_L = \frac{C_0}{1-(1-k)f_S}$, where C_0 is the initial liquid concentration, k is the equilibrium partition coefficient, and f_S is the solid fraction. On the other hand, Gulliver–Scheil model describes the solute redistribution during solidification by assuming complete diffusion in liquid, no diffusion in solid and local equilibrium at the interface.

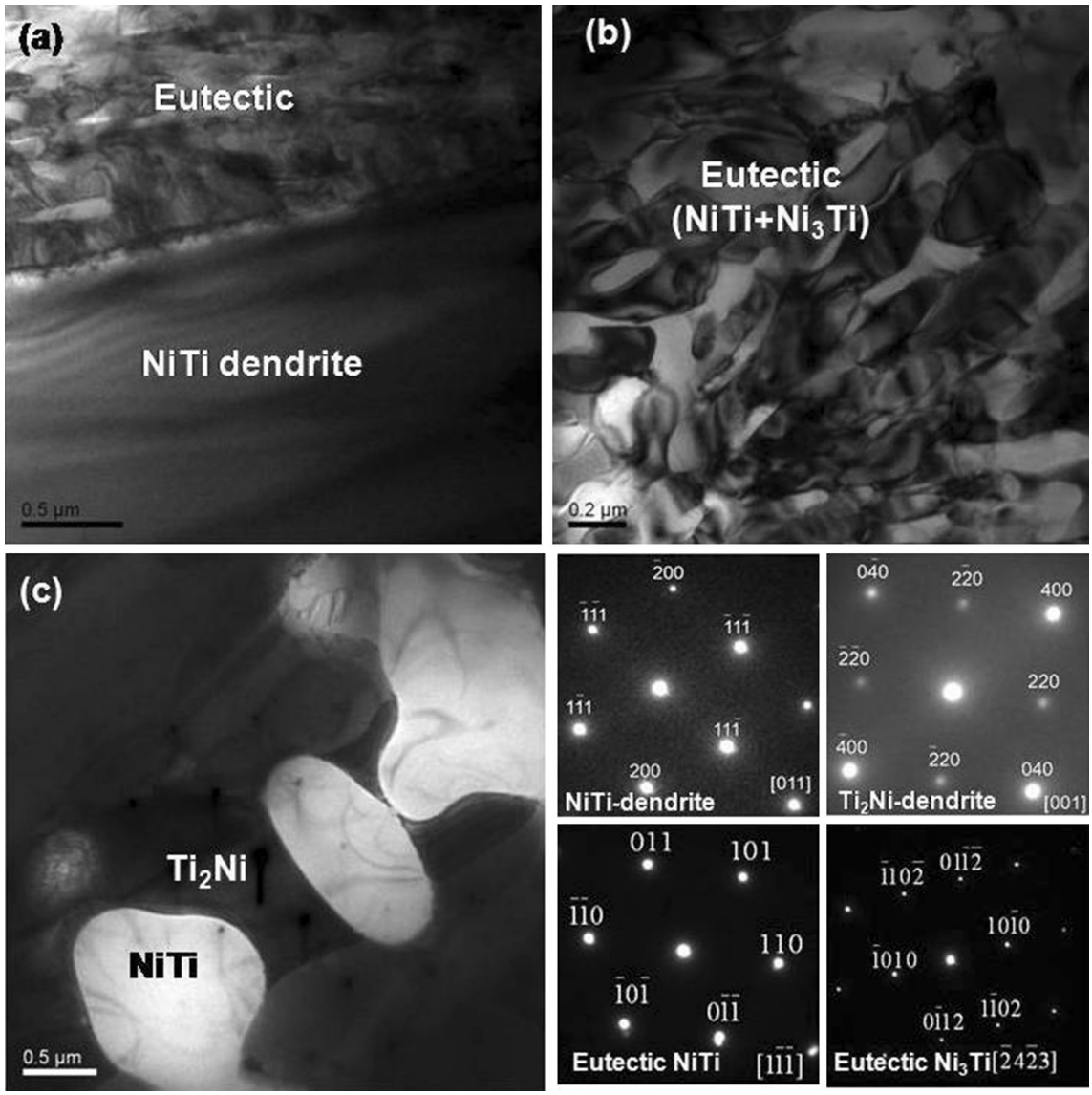

Fig. 6—TEM micrograph of $Ni_{48}Cu_{10}Co_2Ti_{38}Ta_2$ alloy: Bright-field micrograph of (*a*) eutectic lamellae plus NiTi dendrite, (*b*) Eutectics between NiTi and Ni_3Ti and (*c*) micron-sized NiTi and Ti_2Ni phases.

The liquid concentration (C_L) at solid–liquid (S/L) interface can be expressed as $C_L = C_0(1 - f_S)^{k-1}$, where C_0 is the initial liquid concentration, k is the equilibrium partition coefficient, and f_S is the solid fraction. The thermodynamic simulations of the investigated Ni-based alloys are carried out using two preceding models to predict both equilibrium and non-equilibrium solidification pathways, respectively. It is important to note that the industrially processed alloys follow the non-equilibrium solidification pathways due to solute segregation. Therefore, Gulliver–Scheil model is generally used as appropriate model for predicting qualitatively real solidification pathways[37–39] because of the limited solute diffusion in the solid.

According to Lever rule model, the solidification pathways for $Ni_{60}Ti_{40}$ alloy (Figure 7(a)) reveal that the liquid is transformed to form the single NiTi phase (*i.e.*, L → L + NiTi → NiTi) and no other phases precipitate from the liquid, whereas Gulliver–Scheil model shows that, firstly, NiTi phase is evolved from the liquid (*i.e.*, L → L + NiTi) and, subsequently, the remaining liquid leads to the formation of mixture of NiTi and Ni_3Ti phases (*i.e.*, L → NiTi + Ni_3Ti).

Similarly, the solidification pathways following Lever rule model for ternary $Ni_{50}Cu_{10}Ti_{40}$ alloy (shown in Figure 7(b)) reveal that all of the liquid is transformed to form the NiTi phase only (*i.e.,* L → L + NiTi → NiTi). However, Gulliver–Scheil model shows the corresponding solidification pathways for studied ternary alloy implies that, at first, NiTi phase is formed from the liquid, then secondary phase Ni_3Ti is precipitated from the remaining liquid, and finally, a small fraction of Cu_2Ti phase is evolved during the last-stage solidification. This implies that the mixture of NiTi, Ni_3Ti, and small fraction of Cu_2Ti phases is formed from liquid in $Ni_{50}Cu_{10}Ti_{40}$ alloy, *i.e.,* the sequence of solidification is

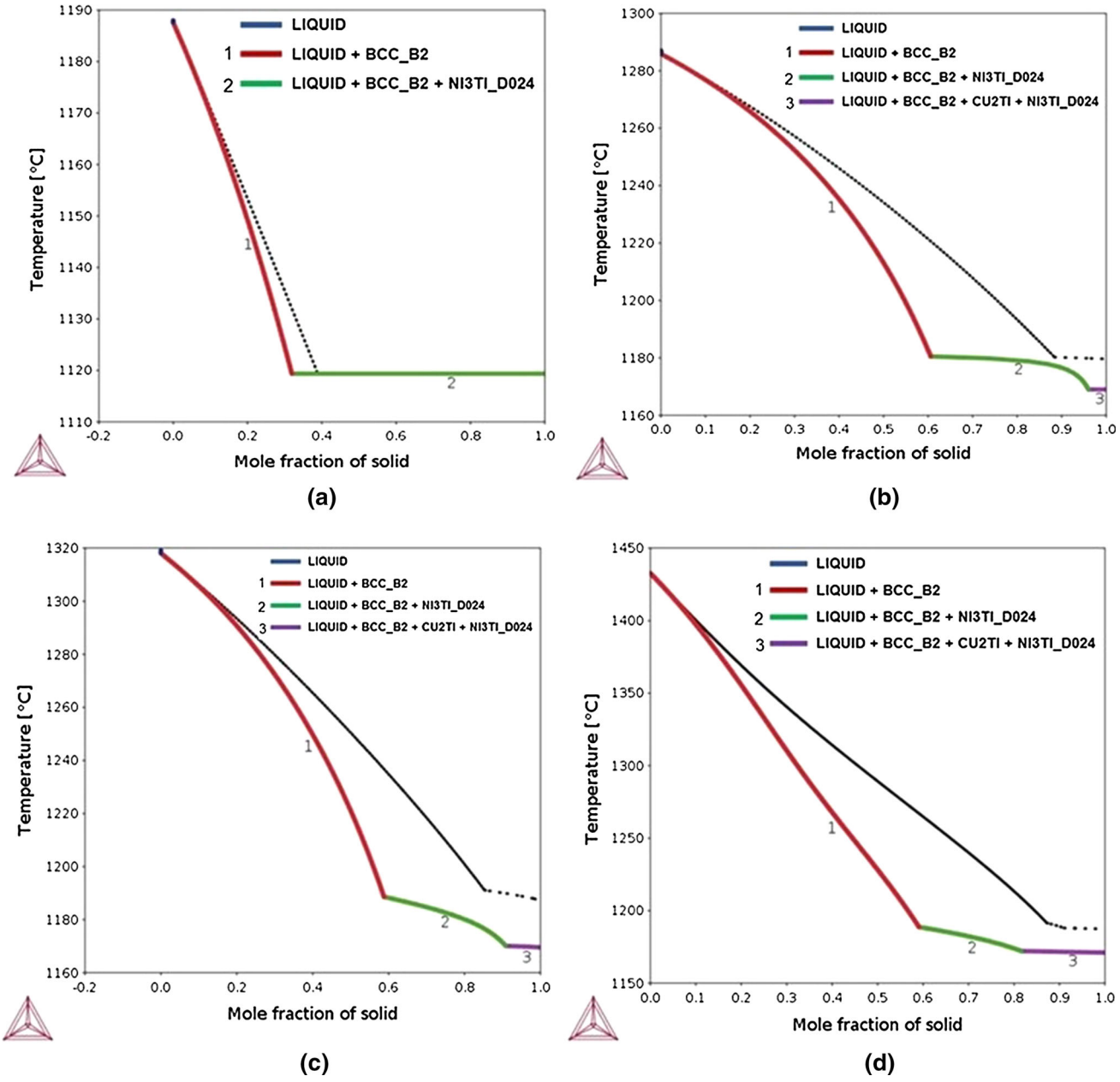

Fig. 7—Plot between mole fraction of solid and temperature (°C) showing simulated solidification pathways of (*a*) $Ni_{60}Ti_{40}$, (*b*) $Ni_{50}Cu_{10}Ti_{40}$, (*c*) $Ni_{48}Cu_{10}Co_2Ti_{40}$, and (*d*) $Ni_{48}Cu_{10}Co_2Ti_{38}Ta_2$ alloys using Lever rule (dotted line) and Gulliver–Scheil models (solid line).

Table II. Detailed Phase Transformation Behavior of the Investigated Ni-Rich Ni-Ti-Based Alloys

Alloys	$Ni_{60}Ti_{40}$	$Ni_{50}Cu_{10}Ti_{40}$	$Ni_{48}Cu_{10}Co_2Ti_{40}$	$Ni_{48}Cu_{10}Co_2Ti_{38}Ta_2$
Evolution of dendrite	$L \rightarrow L + NiTi$	$L \rightarrow L + NiTi$	$L \rightarrow L + NiTi$	$L \rightarrow L + NiTi$
Eutectic reaction	$L \rightarrow NiTi + Ni_3Ti$	$L \rightarrow NiTi + Ni_3Ti$	$L \rightarrow NiTi + Ni_3Ti$	$L \rightarrow NiTi + Ni_3Ti$
Solid-state reaction-I (eutectoid reaction)	$NiTi \rightarrow Ti_2Ni + Ni_3Ti$	$NiTi \rightarrow Ti_2Ni + Ni_3Ti$	$NiTi \rightarrow Ti_2Ni + Ni_3Ti$	$NiTi \rightarrow Ti_2Ni + Ni_3Ti$
Solid-state reaction-II	$NiTi \rightarrow$ R-Phase $\rightarrow$ B19′-Phase	$NiTi \rightarrow$ R-Phase	$NiTi \rightarrow$ R-Phase	no solid-state reaction-II

given as $L \rightarrow L + NiTi \rightarrow L + NiTi + Ni_3Ti \rightarrow L + NiTi + Cu_2Ti + Ni_3Ti \rightarrow NiTi + Cu_2Ti + Ni_3Ti$. The similar type of solidification sequence for quaternary $Ni_{48}Cu_{10}Co_2Ti_{40}$ alloy (Figure 7(c)) and quinary $Ni_{48}Cu_{10}Co_2Ti_{38}Ta_2$ alloy (shown in Figure 7(d)) has been found. It is important to note that the phase prediction by Gulliver–Scheil model is in good agreement with the experimental results for binary alloy. However, the small volume fraction of Cu_2Ti phase has been observed during the last stage of solidification in

the simulated results of ternary, quaternary, and quinary alloys. This discrepancy from the experimental results is attributed to the factor, *i.e.,* there is some diffusion of solutes in the solid in the real solidification process, which is not taken into consideration in the Gulliver–Scheil model. Furthermore, the small volume fraction of Ti_2Ni, R-, and M-phases formed in the studied Ni-based alloys has also not been observed in the simulated results because of the formation of these phases during solid-state transformation which is also being unconsidered in the Gulliver–Scheil model.

It is important to note that the phase formation in binary $Ni_{60}Ti_{40}$ alloy, predicted by Gulliver–Scheil solidification model, is in good agreement with the experimental results, whereas in the case of ternary $Ni_{50}Cu_{10}Ti_{40}$, quaternary $Ni_{48}Cu_{10}Co_2Ti_{40}$, and quinary $Ni_{48}Cu_{10}Co_2Ti_{38}Ta_2$ alloys, the simulated path is in disagreement with the experimental results, since there is some diffusion of solutes in the solid in the real solidification process which is not being considered in the Gulliver–Scheil model.

VI. CONCLUSIONS

The following conclusions can be made based on the extensive electron microscopic studies on the investigated novel Ni-rich Ni-Ti-based alloys:

1. The investigated Ni-rich Ni-Ti-based alloys reveals the presence of ultrafine to nanoscale eutectic (NiTi, Ni_3Ti) with two different kinds of dendritic phases (NiTi, Ti_2Ni) in different alloys. However, the secondary precipitate of Ti_2Ni is observed from binary Ni-Ti alloy to quinary Ni-Cu-Co-Ti-Ta alloy.
2. In the $Ni_{60}Ti_{40}$ binary alloy, the ordered NiTi (B2) phase undergoes solid-state transformation to form the trigonal (R) phase and NiTi martensite phase (M-phase), *i.e.,* B2 $\rightarrow$ R-phase $\rightarrow$ M-phase, whereas in the ternary ($Ni_{50}Cu_{10}Ti_{40}$) and the quaternary ($Ni_{48}Cu_{10}Co_2Ti_{40}$) alloys, the martensitic transformation of the ordered NiTi (B2) dendrites is suppressed. This is attributed to the addition of alloying elements (Cu, Co). However, ordered NiTi (B2) phase is transferred to form only R-phase, *i.e.,* B2 $\rightarrow$ R-phase.
3. Quinary ($Ni_{48}Cu_{10}Co_2Ti_{38}Ta_2$) alloy reveals the disordered NiTi phase and the secondary Ti_2Ni precipitate along with eutectic phases (NiTi and Ni_3Ti).
4. The simulated Gulliver–Scheil solidification pathways for the binary alloy are in good agreement with the experimental results, whereas the experimental results for ternary, quaternary, and quinary alloys deviates from the Gulliver–Scheil simulated path.

REFERENCES

1. R. Lahoz and J.A. Puertolas: *J. Alloy. Compd.*, 2004, vol. 381, pp. 130–36.
2. Y. Liu, Y. Liu, and J.V. Humbeeck: *Acta Mater.*, 1999, vol. 47, pp. 199–209.
3. H. Scherngell and A.C. Kneissl: *Scripta Mater.*, 1998, vol. 39, pp. 205–12.
4. S.A. Shabalovskaya: *Biomed. Mater. Eng.*, 2002, vol. 12, pp. 69–109.
5. K. Otsuka and C.M. Wayman , eds., *Shape Memory Materials*, Cambridge University Press, Cambridge, 1998.
6. G. He, J. Eckert, W. Löser, and L. Schultz: *Nat. Mater.*, 2003, vol. 2, pp. 33–37.
7. J.M. Park, S.W. Sohn, T.E. Kim, K.B. Kim, W.T. Kim, and D.H. Kim: *Scripta Mater.*, 2007, vol. 57, pp. 1153–56.
8. D.V. Louzguine, H. Kato, and A. Inoue: *Philos. Mag. Lett.*, 2004, vol. 84, pp. 359–64.
9. J.M. Park, N. Mattern, U. Kuhn, J. Eckert, K.B. Kim, W.T. Kim, K. Chattopadhyaya, and D.H. Kim: *J. Mater. Res.*, 2009, vol. 24, pp. 2605–09.
10. J. Das, K.B. Kim, F. Baier, W. Löser, A. Gebert, and J. Eckert: *J. Alloy. Compd.*, 2007, vols. 434–435, pp. 28–31.
11. S. Samal, B. Mondal, K. Biswas, and Govind: *Metall. Mater. Trans. A*, 2013, vol. 44A, pp. 427–39.
12. B. Mondal, S. Samal, K. Biswas, and Govind: *IOP Conf. Ser. Mater. Sci. Eng.*, 2011, vol. 27, p. 012025.
13. S. Samal, P. Gautam, S. Agarwal, and K. Biswas: *Mater. Sci. Forum*, 2014, vol. 790, pp. 497–502.
14. S. Samal, S. Agarwal, P. Gautam, and K. Biswas: *Metall. Mater. Trans. A*, 2015, vol. 46A, pp. 851–68.
15. G. He, W. Löser, and J. Eckert: *Acta Mater.*, 2003, vol. 51, pp. 5223–34.
16. G. He, J. Eckert, W. Löser, and M. Hagiwara: *Acta Mater.*, 2004, vol. 52, pp. 3035–46.
17. H.C. Yim, D. Xu, and W.L. Johnson: *Appl. Phys. Lett.*, 2003, vol. 82, pp. 1030–32.
18. H.C. Yim, R.D. Conner, and W.L. Johnson: *Scripta Mater.*, 2005, vol. 53, pp. 1467–70.
19. D. Xu, G. Duan, W.L. Johnson, and C. Garland: *Acta Mater.*, 2004, vol. 52, pp. 3493–97.
20. S. Samal and K. Biswas: *J. Nanopart. Res.*, 2013, vol. 15, pp. 1–11.
21. R. Elliott: *Eutectic Solidification Processing: Crystalline and Glassy Alloys*, Butterworths, London, 1983.
22. L.C. Zhang: *Adv. Mat. Res.*, 2012, vol. 1, pp. 13–29.
23. K.A. Jackson and J.D. Hunt: *Trans. Metall. Soc. AIME*, 1966, vol. 236, pp. 1129–42.
24. R. Trivedi, P. Magnin, and W. Kurz: *Acta Metall. Mater.*, 1987, vol. 35, pp. 971–80.
25. Q.L. Dai, B.B. Sun, M.L. Sui, G. He, Y. Li, J. Eckert, W.K. Luo, and E. Ma: *J. Mater. Res.*, 2004, vol. 19, pp. 2557–66.
26. O. Matsumoto, S. Miyazaki, K. Otsuka, and H. Tamura: *Acta Metall. Mater.*, 1987, vol. 35, pp. 2137–44.
27. K.F. Hane and T.W. Shield: *Acta Mater.*, 1999, vol. 47, pp. 2603–17.
28. K. Otsuka and X. Ren: *Prog. Mater. Sci.*, 2005, vol. 50, pp. 511–678.
29. M.S. Choi, T. Fukuda, T. Kakeshita, and H. Mori: *Phil. Mag.*, 2006, vol. 86, pp. 67–78.
30. M.C. Flemings: *Solidification Processing*, McGraw-Hill, New York, 1974.
31. X. Zhang and H. Sehitoglu: *Mater. Sci. Eng. A*, 2004, vol. 374, pp. 292–302.
32. M.B. Salamon, M.E. Meichle, and C.M. Wayman: *Phys. Rev. B*, 1985, vol. 31, pp. 7306–15.
33. S. Miyazaki and C.M. Wayman: *Acta Metall.*, 1988, vol. 36, pp. 181–92.
34. C.M. Hwang, M.E. Meichle, M.B. Salamon, and C.M. Wayman: *Phil. Mag. A*, 1983, vol. 47, pp. 31–62.
35. P.J.S. Buenconsejo, R. Zarnetta, and A. Ludwig: *Scripta Mater.*, 2011, vol. 64, pp. 1047–50.
36. J.A. Dantzig and M. Rappaz: *Solidification*, EPFL Press, Lausanne, 2009, pp. 345–427.
37. Q. Zuo, F. Liu, L. Wang, and C. Chen: *Metall. Mater. Trans. A*, 2013, vol. 44A, pp. 3014–27.
38. K. Biswas, G. Phanikumar, D.-H. Moritz, D.M. Herlach, and K. Chattopadhyaya: *Phil. Mag.*, 2007, vol. 87, pp. 3817–37.
39. K. Biswas, G. Phanikumar, K. Chattopadhyaya, T. Volkmann, O. Funke, D.-H. Moritz, and D.M. Herlach: *Mater. Sci. Eng. A*, 2004, vols. 375–377, pp. 464–67.